Title: Resting-state fMRI-based screening of deschloroclozapine in rhesus macaques predicts dosage-dependent behavioral effects

Authors: Atsushi Fujimoto[1]*, Catherine Elorette[1]*, J. Megan Fredericks[1], Satoka H. Fujimoto[1], Lazar Fleysher[4], Peter H. Rudebeck[1+], and Brian E. Russ[1,2,3+y]

Author affiliations:

[1] Nash Family Department of Neuroscience and Friedman Brain Institute, Icahn School of Medicine at Mount Sinai, One Gustave L. Levy Place, New York, NY 10029

[2] Center for Biomedical Imaging and Neuromodulation, Nathan Kline Institute, 140 Old Orangeburg Road, Orangeburg, NY 10962

[3] Department of Psychiatry, New York University at Langone, One, 8, Park Ave, New York, NY 10016

[4] BioMedical Engineering and Imaging Institute, Icahn School of Medicine at Mount Sinai, One Gustave L. Levy Place, New York, NY 10029

* These authors contributed equally to this work

+ Joint last author

y Corresponding author

Correspondence:

Brian E. Russ

brian.russ@mssm.edu

Running title: fMRI-based screening of deschloroclozapine in macaques

Key words: resting-state fMRI; functional connectivity; independent component analysis; chemogenetics; deschloroclozapine; rhesus macaque

ABSTRACT

Background: Virally-mediated chemogenetic techniques hold the promise of circuit-specific neuromodulation for human brain disorders. Their protracted development in primates and issues related to the specificity of the actuator drugs has significantly slowed their implementation. Here we took a multi-disciplinary approach to assessing the translational appropriateness of a newly identified actuator drug, deschloroclozapine (DCZ).

Methods: Resting-state functional MRI (rs-fMRI) data was acquired from seven rhesus macaques (6 males and 1 female) after administration of either vehicle, 0.1 or 0.3 mg/kg DCZ, the latter of which produce 80% and near 100% chemogenetic receptor occupancy, respectively. Seed-based comparative-connectome analysis and independent component analysis assessed dose dependent neural impact. Two subsets of subjects were tested on socio-emotional tasks (N = 4), and a probabilistic learning task (N = 3), assessing DCZ's impact on unconditioned and conditioned affective responses, respectively.

Results: Neither vehicle nor 0.1 mg/kg DCZ changed overall functional connectivity, affective responses, or reaction times in the learning task. 0.3 mg/kg DCZ increased functional connectivity, particularly in frontal regions, and increased reaction times in the learning task. Notably, there was a positive correlation between changes in overall functional connectivity and reaction time.

Conclusions: These experiments show the utility of rs-fMRI for *in-vivo* drug screening and benchmarking. We found that low dose DCZ does not alter brain function or affective behavior. However, higher doses of DCZ impacts frontal connectivity and is associated with deficits in task execution. Implementation of these methods will accelerate the development of chemogenetic in primates for research and therapeutic approaches.

INTRODUCTION

The development of chemogenetics such as Designer Receptors Exclusively Activated by Designer Drugs (DREADDs) has ushered in a new era of neuroscience research in animal models. DREADDs utilize a family of modified G-protein coupled muscarinic cholinergic receptors to either increase, decrease, or produce bursts of neural activity *in vivo* (1). In rodents, DREADDs have been instrumental for identifying the function of specific cell populations and neural circuits (2, 3). The development of DREADDs in primates has been slower for a number of reasons (4), but holds the promise of enabling the translation of chemogenetic methods to treat psychiatric and neurological disorders.

At the cellular level, DREADD receptors alter the membrane potential of neurons only when bound by non-endogenous ligands (2). Recently, deschloroclozapine (DCZ) has been identified as a selective and high-affinity activator for muscarinic-based DREADDs with few off-target effects, unlike the original actuator clozapine-N-oxide (5, 6). At a dose of 0.1mg/kg, DCZ occupies up to 80% of DREADD receptors *in vivo* (5). This dose level produces rapid and robust changes in neural activity and induces alterations in behavior when DREADD receptors are present. Despite this, there are open questions that could limit the appropriateness of DCZ for use in both basic and clinical settings.

First, it is unclear how DCZ impacts brain-wide patterns of neural activity. This is potentially essential for discerning the more subtle effects of systemic DCZ on the brain, such as changes in functional connectivity between brain areas. Second, while it is known that a functional dose of 0.1 mg/kg DCZ has little impact on tasks that assess executive function or motivation (5, 7), it is unknown if the same dose causes changes in translationally relevant affective tasks. While DCZ has negligible affinity for most endogenous receptors, it has some affinity to muscarinic acetylcholine receptors (mAchR) and potentially more importantly for affective behaviors, serotonin type-2 receptors (5) that are primarily located in the cortex (8, 9). It is possible therefore that even at low, but functionally relevant, doses DCZ may be able to impact affective behavior by binding to these endogenous receptors. Addressing these issues in macaque monkeys is critical as

marked changes in brain-wide activity patterns, behavior or both would limit the usefulness of DCZ as the actuator in basic neuroscience and in future clinical settings.

Here we addressed these questions using resting-state functional magnetic resonance imaging (rs-fMRI) and behavioral assessments in macaque monkeys. We measured the impact of either vehicle, low-dose DCZ (0.1 mg/kg), or high-dose DCZ (0.3 mg/kg) on whole-brain fMRI resting-state functional connectivity as well as in conditioned and unconditioned tasks that assess socio-emotional processing. We found no changes in overall functional connectivity or affective behavior after administration of vehicle or 0.1 mg/kg of DCZ. Conversely, higher doses of DCZ at 0.3 mg/kg affected brain-wide patterns of functional connectivity, in particular in the connections of frontal regions to temporal and parietal lobes. This dose level also impacted decision-making in a probabilistic learning task, increasing reaction times. Thus, our experiments reveal the dosage-dependent impact of DCZ on brain-wide functional connectivity and demonstrate the potential value of rs-fMRI as an additional drug-screening tool in basic and potentially clinical neuroscience.

METHODS AND MATERIALS

Subjects

Seven adult rhesus macaques (*Macaca mulatta*) served as subjects (6 males and 1 female). All subjects underwent anesthetized functional MRI scans, while subsets of 4 and 3 animals were assessed in 2 socio-emotional tasks and a probabilistic learning task, respectively (see **Supplemental Table 1**). All procedures were reviewed and approved by the Icahn School of Medicine Animal Care and Use Committee.

Resting-state fMRI experiments

Animals were first sedated with ketamine (5 mg/kg) and dexmedetomidine (0.0125 mg/kg), and then intubated and maintained under low level (0.7-0.8 %) isoflurane anesthesia throughout a session (10). Either

96 vehicle (2% DMSO in saline), low-dose DCZ (0.1 mg/kg), or high-dose DCZ (0.3 mg/kg) was administered
97 intravenously halfway through a session. In each session, three to four runs of echo planar image (EPI)
98 functional scans (1.6 mm isotropic, TR/TE 2120/16 ms, flip angle 45°, 300 volumes per each run) were
99 obtained for both before ('baseline' scans) and after drug injection ('test' scans) (**Figure 1**).

100 *Behavioral experiments*

101 Four animals were assessed in the human intruder task (11) and social interaction tests (12). Either vehicle
102 or low-dose DCZ was administered intramuscularly 30-60 minutes prior to a test. Experiments were
103 counterbalanced for treatment order among animals.

104 Three monkeys were assessed in a probabilistic learning task on a touch-sensitive monitor. In this task,
105 subjects had to learn to discriminate which visual stimulus in two pairs of novel stimuli was associated with
106 the highest probability (80 or 20%) of receiving a food reward. Each session consisted of 200 trials.

107 *Data analyses*

108 The connectome analyses were computed using the 3dNetCorr function in AFNI (13, 14). We computed
109 the correlation between anatomical ROIs at various levels of the cortical (15) and subcortical (16)
110 hierarchical atlases. The correlation matrices, or connectomes, were Fisher's z-transformed and then
111 averaged within condition (both baseline and test for: vehicle, low-dose DCZ, and high-dose DCZ). We
112 calculated the difference between connectomes by subtracting the baseline data from the test data for each
113 condition. We also performed a modified group Independent Components Analysis (ICA) using FSL's
114 melodic ICA function (17, 18), allowing for 30 possible components. The extracted IC scores were then
115 submitted to a 2 (baseline or test scan) by 3 (vehicle, low-dose DCZ, or high-dose DCZ) ANOVA which
116 was computed on a voxel-by-voxel basis.

117 Data from unconditioned socio-emotional tests were scored in Observer XT by a scorer blinded to the
118 condition and analyzed using GraphPad Prism (GraphPad, San Diego CA). Behavioral ethograms
119 (**Supplemental Tables 2** and **3**) were adapted from previous studies (19, 20). Social interaction was

analyzed via paired t-test; human intruder was analyzed via repeated measures two-way ANOVA with factors of drug and trial type as main factors and monkey as a random effect. Data from the probabilistic learning task was analyzed using MATLAB. We assessed reaction time (RT, defined as the time duration from stimuli presentation to a choice response) as a measure of general task-execution processes such as attention or motivation. The effect of drug on RT was assessed using an ANOVA with factors of drug as a main effect and monkey and session as random effects.

For details of experimental procedures and analyses, see *Supplemental Information*.

RESULTS

The impact of low- and high-dose DCZ on brain-wide fMRI functional connectivity

Seven subjects were lightly anesthetized and underwent functional MRI scanning (**Figure 1**). To assess the changes in brain-wide functional connectivity following DCZ administration, we first took a seed-based functional connectivity approach using predetermined regions of interest (ROIs) that were based on the cortical hierarchical atlas (CHARM) (15) and subcortical hierarchical atlas (SARM) (16) for rhesus macaques (**Figure 2A** and **C**). The correlation coefficients between fMRI signal time courses in all ROIs were standardized for each subject and a matrix of z-transformed values was computed for each condition, for both the baseline (before drug injection) and test (after drug injection) scans (**Figure 2B** and **D**, left and center columns). Then, the difference in z-value (subtraction from test to baseline data) was computed for each drug condition (**Figure 2B** and **D**, right columns). Taking this approach allowed us to control for session-to-session variation in fMRI signals that could influence the results. Figure 2 shows the full matrix of correlation coefficients from this connectome-based analysis from a single subject (monkey Bu). As expected, we found clear patterns of correlations between distinct brain areas that are consistent to previous reports in macaques (21) in baseline scans (**Figure 2B**, left column).

143 Neither vehicle (2% DMSO in saline) nor low-dose DCZ (0.1 mg/kg) administration caused a detectable
144 change in the overall pattern of functional connectivity and consequently there were very minor differences
145 in functional connectivity between test and baseline scans for these conditions (**Figure 2B**, compare top-
146 right and middle-right panels). Conversely, high-dose DCZ administration (0.3 mg/kg) profoundly
147 increased functional connectivity across cortical regions (**Figure 2B**, bottom-right panel). This effect was
148 most apparent in frontal areas, compared to baseline where correlations within frontal regions increased, as
149 well as between frontal cortex and other parts of the brain. In contrast to cortex, correlations between
150 subcortical areas were not impacted by the different levels of drug (**Figure 2D**).

151 To assess the impact of DCZ on brain-wide connectomes at the group level, we computed correlation
152 matrices for individual subjects for baseline and test scans (N = 5-6 subjects per condition, see
153 **Supplemental Table 1**). Then the difference in z-values (test - baseline) were averaged across subjects
154 (**Figure 3**). Similar to what we saw for a single subject (**Figure 2**), vehicle or low-dose DCZ administration
155 had little impact on overall functional connectivity either in cortical or subcortical areas. In contrast, high-
156 dose DCZ generally increased functional connectivity in cortical areas but not in subcortical areas (**Figure**
157 **3A** and **D**). Collectively, averaged functional connectivity was stronger in the high-dose DCZ condition
158 compared to the vehicle or low-dose DCZ condition in cortical areas but not in subcortical areas (**Figure**
159 **3B** and **E**). Two-way ANOVA (Drug: vehicle, low-dose DCZ, or high-dose DCZ × Area category: cortical
160 or subcortical areas) revealed significant main effects of drug ($F_{2,13450} = 31$, $p = 0.0001$) and an interaction
161 between drug and area category ($F_{2,13450} = 8.2$, $p = 0.016$). Further post-hoc analyses confirmed that high-
162 dose DCZ modulated overall functional connectivity predominantly in cortical areas (vehicle or low-dose
163 DCZ versus high-dose DCZ, $p < 0.0001$).

164 Next we assessed how high-dose DCZ differentially impacts functional connectivity across the different
165 lobes of the brain. The regions that showed marked changes in functional connectivity between high-dose
166 DCZ and vehicle conditions were mainly located in frontal, temporal, parietal, but not in occipital cortex
167 (**Figure 3C**, bottom, * denotes rank-sum test $p < 0.01$ with Bonferroni correction). Furthermore, the

168 proportion of brain areas that were impacted by low-dose DCZ was far lower than those impacted by high-
169 dose DCZ (**Figure 3C**, top). A subsequent chi-square test showed that the difference in the proportions of
170 areas impacted was significantly different between low-dose and high-dose DCZ ($\chi^2 = 23$, $p = 1.6 \times 10^{-6}$).
171 Neither dose level of DCZ affected functional connectivity in subcortical areas (**Figure 3F**), suggesting the
172 mechanism of functional-connectivity changes was exclusive to cortical regions.

173 *Independent-components reflect brain-wide functional-connectivity changes caused by high-dose DCZ*

174 While informative, the prior seed-based approach is limited by predefined anatomical boundaries and may
175 overlook relevant changes in MRI signals specifically induced by high-dose DCZ. Also, the seed-based
176 approach does not reveal network-level changes that includes more than two areas. Thus, we next performed
177 a data-driven independent-component analysis (ICA) to identify 30 independent components (ICs) that are
178 spatially coherent time courses in the whole-brain fMRI signal. We found a variety of ICs mainly located
179 in cortical areas (**Figure 4A-F**, top). To identify ICs, and thus regions that are affected by high-dose DCZ,
180 a two-way ANOVA was performed (Drug: vehicle, low-dose DCZ or high-dose DCZ × Time: baseline or
181 test). This analysis revealed clusters (> 60 voxels with $F > 3.5$) in a subset of the ICs that showed a
182 significant main effect of drug; these included cortical areas such as the dorso-lateral prefrontal cortex
183 (dlPFC), anterior cingulate cortex (ACC), posterior cingulate cortex (PCC), ventromedial cortex (vmPFC),
184 somatosensory and motor cortices (**Figure 4A-F**, bottom). Notably, IC 3 showed an effect of drug on the
185 fronto-temporo-parietal network which is implicated in mediating attentional processes (22) (**Figure 4A**).
186 Further, the ICs which showed drug effects overlapped with regions that showed increased functional
187 connectivity in our ROI based analyses (**Figure 3**). Thus, systemic administration of high-dose DCZ
188 influenced brain-wide spatially coherent patterns of neural activity, especially in attentionally-linked
189 fronto-temporo-parietal circuits.

190 *Negligible effects of low-dose DCZ on socio-emotional behaviors*

191 Our imaging results demonstrated a negligible impact of 0.1 mg/kg DCZ on brain-wide functional
192 connectivity with the least impact in subcortical structures (**Figure 3**). Although no adverse effects of low-
193 dose DCZ were reported in a working-memory task in macaque monkeys (5, 7), no study has examined the
194 impact of DCZ on the socio-emotional responses of monkeys. To address this issue, a subset of 4 subjects
195 were first assessed in the human intruder task, a well-validated socio-emotional task for non-human
196 primates. Subjects received a systemic injection (i.m.) of either 0.1 mg/kg DCZ or vehicle solution prior to
197 testing. We analyzed the time spent motionless on each trial type (alone, profile, or stare condition) as a
198 measure of anxiety-like behavior. Based on previous reports, we expected that the animals spent more time
199 motionless in the 'profile' condition in response to indirect threat compared to the 'alone' or directly
200 threatening 'stare' condition (11). As expected, animals spent more time motionless in the 'profile' condition
201 in both vehicle and low-dose DCZ conditions (**Figure 5A**). A two-way ANOVA matched for subject (Trial
202 type: alone, profile or stare × Drug: vehicle or low-dose DCZ) revealed a significant main effect of trial
203 type ($F_{1,3} = 16$, $p = 0.049$), but no main effect of drug ($F_{1,3} = 0.24$, $p = 0.66$) nor an interaction between
204 trial type and drug ($F_{2,6} = 1.4$, $p = 0.32$).

205 We also examined whether low-dose DCZ alters social interaction. For this test, subjects were paired with
206 a cagemate, and the total social contact, which comprises grooming, play, and passive physical contact
207 between partners, was measured (12). Based on these measures of social interaction, there were no
208 statistical differences between vehicle and low-dose DCZ conditions (Mean ± SD, vehicle: 435.4 ± 198.2 s
209 and low-dose DCZ: 502.1 ± 342.3 s, respectively; $t = 0.26$, $p = 0.81$, paired t-test). Thus, we found no
210 evidence that the socio-emotional functions of macaque monkeys were affected by systemic administration
211 of low-dose DCZ across tasks.

212 *The effect of high-dose DCZ on decision-making and its relation to resting-state functional connectivity*

213 Our imaging results revealed an increase in overall functional connectivity in cortical areas following a
214 systemic administration of high-dose DCZ (0.3 mg/kg) (**Figures 3** and **4**). Because the changes occurred
215 mainly in frontal, temporal and parietal cortex, it may influence behaviors that are dependent on functional

interaction between these areas (**Figure 4**). To test this, we trained a subset of 3 monkeys in a translationally-relevant probabilistic learning task that relies on frontal and temporal cortices (23-25). Here we theorized that high-dose DCZ would specifically impact monkeys' reaction time (RT) as the drug slow decision-making. As expected, RT increased after high-dose DCZ but not low-dose DCZ compared to the vehicle condition (**Figure 5B**). A one-way repeated measures ANOVA (Drug: vehicle, low-dose DCZ or high-dose DCZ) revealed a significant main effect of drug ($F_{2,49} = 17$, $p = 2.5 \times 10^{-6}$), suggesting that high-dose DCZ causes an impairment in general task-execution processes, while low-dose DCZ did not.

To analyze the relationship between the neural and behavioral effects following systemic DCZ administration, we performed a correlation analysis between overall functional-connectivity changes in cortical (**Figure 5C**, left) or subcortical areas (**Figure 5C,** right) and RT in the 3 animals. There was a significant positive correlation between RT and overall cortical functional connectivity ($n = 58$, $p = 0.023$) but no correlation with subcortical areas ($n = 58$, $p = 0.49$). Thus, cortical resting-state functional-connectivity changes following DCZ administration were related to the impairment in task-execution process observed after high-doses of DCZ.

DISCUSSION

To assess the impact of DCZ on brain-wide function in primates, we conducted a resting-state fMRI (rs-fMRI) experiments and behavioral assessments in macaque monkeys. We found that systemic administration of low-dose DCZ, 0.1 mg/kg, did not affect overall functional connectivity or the socio-emotional behaviors we measured. However, we did find that systemic administration of high-dose DCZ, 0.3 mg/kg, increased overall cortical functional connectivity, and was associated with slowed responses in a probabilistic learning task. Taken together, our data indicate that at a functionally effective dose of 0.1 mg/kg, DCZ appears to be appropriate for use as a DREADD actuator in non-human primates, a key finding if chemogenetics are to be translated further.

240 *Negligible impact of low-dose DCZ on brain-wide functional connectivity or socio-emotional behaviors*

241 Although DCZ was identified as a potent, selective, and metabolically stable DREADD actuator (5), prior
242 work only showed its local effects on the brain using electrophysiology and [18F] FDG-PET imaging (5).
243 What is not clear is if it impacts brain-wide neural activity in normal controls where DREADD receptors
244 are not present. Consequently, we conducted an rs-fMRI experiment with seven rhesus monkeys and
245 assessed the effect of different dose levels of DCZ. We hypothesized that 0.1 mg/kg DCZ, which has been
246 shown to be functionally effective in chemogenetic experiments in non-human primates (5, 26), does not
247 affect resting-state functional connectivity. As we expected, low-dose DCZ did not alter brain-wide
248 functional connectivity either in cortical or subcortical areas (**Figures 2** and **3**).

249 Although DCZ has a high-degree of selectivity to DREADD receptors, it shows some affinity to
250 endogenous muscarinic acetylcholine receptors (mAchR) and serotonin receptors (5). Past studies
251 demonstrated a negligible effect of 0.1 mg/kg DCZ on performance in a working-memory task in control
252 monkeys (5, 7), suggesting that this dose of DCZ does not affect working memory performance or attention,
253 processes that are linked to mAchR (27). In the current study, we assessed socio-emotional functions of
254 monkeys in the human intruder and social interaction tasks (11, 12), which are likely mediated by the
255 serotonergic system (28-31). Thus, we asked whether even subtle agonism to endogenous serotonin
256 receptors by DCZ might impact unconditioned affective behaviors. The current results indicate that
257 systemic administration of low-dose DCZ did not strengthen or attenuate affective behaviors of monkeys
258 (**Figure 5**). In summary, there is a negligible effect of low-dose DCZ on socio-emotional functions or brain-
259 wide functional connectivity.

260 *Functional-connectivity changes following high-dose DCZ administration*

261 Systemic administration of the higher dose of 0.3 mg/kg DCZ occupies nearly 100% of DREADD receptors
262 when administered in monkeys expressing DREADDs in their brain (5). Despite this, the question remained
263 as to whether high-dose DCZ may also cause non-specific binding to endogenous receptors and lead to

264 neural and behavioral alterations. Indeed, DCZ at this dosage reduces performance in a working-memory
265 task, suggesting that the excess DCZ affects neural activity (7). Our imaging results revealed that high-dose
266 DCZ caused a prominent increase in overall resting-state functional connectivity between frontal, temporal
267 and parietal lobes that was not observed when vehicle or low-dose DCZ was administered (**Figures 2** and
268 **3**). Notably, the changes were mainly observed in networks that include frontal regions, and no obvious
269 effects were observed in occipital cortex or subcortical structures. This coincides with the pattern of
270 serotonin type-2 receptor (5-HT_{2A}, 5-HT_{2C}) expression in the brain (32, 33), suggesting that excess DCZ
271 may alter brain function through binding to endogenous serotonin receptors.

272 *Behavioral changes following high-dose DCZ administration were associated with functional connectivity*
273 *changes*

274 While low-dose DCZ has little impact on behavior, higher dose levels were associated with behavioral
275 changes. Specifically, high-dose DCZ significantly increased RT in the probabilistic learning task
276 compared to other drug conditions, indicating an impairment in general task-execution processes, such as
277 attention (**Figure 5**). Indeed, our ICA results revealed a prominent drug effect in a fronto-temporo-parietal
278 network (IC 3, **Figure 4**), a network heavily linked to attentional processes (22). Alternatively, high-dose
279 DCZ may increase RT by affecting motivation; this seems less likely, as motivation is largely mediated by
280 subcortical circuits including striatum and midbrain nuclei (34).

281 Moreover, changes in overall resting-state functional connectivity and RT were positively correlated in
282 cortical areas but not in subcortical areas (**Figure 5**). Thus, increases in functional connectivity in cortical
283 areas were associated with the slowing of responding. This result may seem counterintuitive as one could
284 expect an improvement in task performance as a result of increased functional connectivity. However,
285 resting-state fMRI functional connectivity reflects low-frequency fluctuations of neural activity between
286 brain regions, and broad, multi-region, increases in functional connectivity do not necessarily benefit
287 coordinated activity across distributed areas (35). Our data suggests that hyperconnectivity in frontal

288 regions could underlie the impairments in attention that are prominent in neurological and psychiatric
289 disorders (36-38).

290 *Resting-state MRI as a tool for benchmarking in chemogenetic experiments and drug screening*

291 The development of chemogenetic techniques in primates has been relatively slow for a number of reasons,
292 including the limited number of animals available for development and physiological differences between
293 rodents and primates that hampers viral delivery (4, 39). Although past studies demonstrated the usefulness
294 of PET imaging in the quantification of chemogenetic techniques *in vivo* (5, 40-42), the more readily
295 available rs-fMRI has the potential to play a complementary role. As we show here, rs-fMRI provides
296 insight into the correlated patterns of neural activity across distinct brain areas and how this can be impacted
297 by pharmacological agents, a level of analysis unavailable with PET. Thus, rs-fMRI has advantages for
298 screening chemogenetic actuators in naive animals without specific task training. Moreover, rs-fMRI is
299 potentially useful for "benchmarking" the selectivity and potency of novel chemogenetic actuators (43),
300 which may accelerate the development of chemogenetics in primates.

301 *Conclusion*

302 The present study demonstrated that DCZ is inert in non-DREADD monkeys both in brain-wide activity
303 and in conditioned and unconditioned behaviors, if the dosage is carefully controlled. Our study also
304 highlights a link between resting-state hyperconnectivity and behavioral impairments caused by excess
305 DCZ, providing a neural mechanism underlying the side-effects caused by inappropriate use of DCZ. Our
306 data also highlight the translational value of fMRI for helping to accelerate the development of
307 chemogenetics in primates, research that is essential for the translation of these approaches to treat human
308 psychiatric disorders.

309

310 **ACKNOWLEDGEMENTS**

AF, CE, BER and PHR are supported by grants from NIMH and the BRAIN initiative (R01MH110822 and R01MH117040). BER is supported by grants from NIMH (R01MH111439) and NINDS (R01NS109498). AF is supported by Overseas Research Fellowship from Takeda Science Foundation and a Brain & Behavior Research Foundation Young Investigator grant (#28979). We would like to thank Dr Paula Croxson for providing the foundation on which this work was built and Jairo Munoz and Niranjana Bienkowska for assistance with data acquisition. For help with fMRI data pre-processing and analysis we thank Drs Paul Taylor and Alex Franco, respectively.

DISCLOSURES

None.

REFERENCES

1. Armbruster BN, Li X, Pausch MH, Herlitze S, Roth BL (2007): Evolving the lock to fit the key to create a family of G protein-coupled receptors potently activated by an inert ligand. *Proceedings of the National Academy of Sciences of the United States of America*. 104:5163-5168.

2. Roth BL (2016): DREADDs for Neuroscientists. *Neuron*. 89:683-694.

3. Stachniak TJ, Ghosh A, Sternson SM (2014): Chemogenetic synaptic silencing of neural circuits localizes a hypothalamus→midbrain pathway for feeding behavior. *Neuron*. 82:797-808.

4. Fredericks JM, Fujimoto A, Rudebeck PH (2019): Trust, but verify: A cautionary tale of translating chemogenetic methods (A commentray on Galvan et al). *The European journal of neuroscience*. 50:2751-2754.

5. Nagai Y, Miyakawa N, Takuwa H, Hori Y, Oyama K, Ji B, et al. (2020): Deschloroclozapine, a potent and selective chemogenetic actuator enables rapid neuronal and behavioral modulations in mice and monkeys. *Nature neuroscience*. 23:1157-1167.

335 6. Gomez JL, Bonaventura J, Lesniak W, Mathews WB, Sysa-Shah P, Rodriguez LA, et al. (2017):
336 Chemogenetics revealed: DREADD occupancy and activation via converted clozapine. *Science (New*
337 *York, NY)*. 357:503-507.
338 7. Upright NA, Baxter MG (2020): Effect of chemogenetic actuator drugs on prefrontal cortex-
339 dependent working memory in nonhuman primates. *Neuropsychopharmacology : official publication of*
340 *the American College of Neuropsychopharmacology*. 45:1793-1798.
341 8. Barnes NM, Sharp T (1999): A review of central 5-HT receptors and their function.
342 *Neuropharmacology*. 38:1083-1152.
343 9. Varastet M, Brouillet E, Chavoix C, Prenant C, Crouzel C, Stulzaft O, et al. (1992): In vivo
344 visualization of central muscarinic receptors using [11C]quinuclidinyl benzilate and positron emission
345 tomography in baboons. *European journal of pharmacology*. 213:275-284.
346 10. Wu TL, Mishra A, Wang F, Yang PF, Gore JC, Chen LM (2016): Effects of isoflurane anesthesia
347 on resting-state fMRI signals and functional connectivity within primary somatosensory cortex of
348 monkeys. *Brain and behavior*. 6:e00591.
349 11. Kalin NH, Shelton SE (1989): Defensive behaviors in infant rhesus monkeys: environmental cues
350 and neurochemical regulation. *Science (New York, NY)*. 243:1718-1721.
351 12. Kling A, Cornell R (1971): Amygdalectomy and social behavior in the caged stump-tailed
352 macaque (Macaca speciosa). *Folia primatologica; international journal of primatology*. 14:190-208.
353 13. Cox RW (1996): AFNI: software for analysis and visualization of functional magnetic resonance
354 neuroimages. *Computers and biomedical research, an international journal*. 29:162-173.
355 14. Taylor PA, Saad ZS (2013): FATCAT: (an efficient) Functional and Tractographic Connectivity
356 Analysis Toolbox. *Brain connectivity*. 3:523-535.
357 15. Jung B, Taylor PA, Seidlitz J, Sponheim C, Perkins P, Ungerleider LG, et al. (2021): A
358 comprehensive macaque fMRI pipeline and hierarchical atlas. *NeuroImage*. 235:117997.
359 16. Hartig R, Glen D, Jung B, Logothetis NK, Paxinos G, Garza-Villarreal EA, et al. (2021): The
360 Subcortical Atlas of the Rhesus Macaque (SARM) for neuroimaging. *NeuroImage*. 235:117996.

361 17. Beckmann CF, Mackay CE, Filippini N, Smith SM (2009): Group comparison of resting-state
362 FMRI data using multi-subject ICA and dual regression. *NeuroImage*. 47:S148.
363 18. Beckmann CF, Smith SM (2004): Probabilistic independent component analysis for functional
364 magnetic resonance imaging. *IEEE transactions on medical imaging*. 23:137-152.
365 19. Raper J, Murphy L, Richardson R, Romm Z, Kovacs-Balint Z, Payne C, et al. (2019):
366 Chemogenetic Inhibition of the Amygdala Modulates Emotional Behavior Expression in Infant Rhesus
367 Monkeys. *eNeuro*. 6.
368 20. Forcelli PA, Wellman LL, Malkova L (2017): Blockade of glutamatergic transmission in the
369 primate basolateral amygdala suppresses active behavior without altering social interaction. *Behavioral*
370 *neuroscience*. 131:192-200.
371 21. Grayson DS, Bliss-Moreau E, Machado CJ, Bennett J, Shen K, Grant KA, et al. (2016): The
372 Rhesus Monkey Connectome Predicts Disrupted Functional Networks Resulting from Pharmacogenetic
373 Inactivation of the Amygdala. *Neuron*. 91:453-466.
374 22. Sani I, McPherson BC, Stemmann H, Pestilli F, Freiwald WA (2019): Functionally defined white
375 matter of the macaque monkey brain reveals a dorso-ventral attention network. *eLife*. 8.
376 23. Pizzagalli DA, Iosifescu D, Hallett LA, Ratner KG, Fava M (2008): Reduced hedonic capacity in
377 major depressive disorder: evidence from a probabilistic reward task. *Journal of psychiatric research*.
378 43:76-87.
379 24. Rudebeck PH, Saunders RC, Lundgren DA, Murray EA (2017): Specialized Representations of
380 Value in the Orbital and Ventrolateral Prefrontal Cortex: Desirability versus Availability of Outcomes.
381 *Neuron*. 95:1208-1220.e1205.
382 25. Chau BK, Sallet J, Papageorgiou GK, Noonan MP, Bell AH, Walton ME, et al. (2015):
383 Contrasting Roles for Orbitofrontal Cortex and Amygdala in Credit Assignment and Learning in
384 Macaques. *Neuron*. 87:1106-1118.

385 26. Hirabayashi T, Nagai Y, Hori Y, Inoue KI, Aoki I, Takada M, et al. (2021): Chemogenetic
386 sensory fMRI reveals behaviorally relevant bidirectional changes in primate somatosensory network.
387 *Neuron*. 109:3312-3322.e3315.
388 27. Kuczewski N, Aztiria E, Gautam D, Wess J, Domenici L (2005): Acetylcholine modulates
389 cortical synaptic transmission via different muscarinic receptors, as studied with receptor knockout mice.
390 *The Journal of physiology*. 566:907-919.
391 28. Broekkamp CL, Berendsen HH, Jenck F, Van Delft AM (1989): Animal models for anxiety and
392 response to serotonergic drugs. *Psychopathology*. 22 Suppl 1:2-12.
393 29. Weinberg-Wolf H, Chang SWC (2019): Differences in how macaques monitor others: Does
394 serotonin play a central role? *Wiley interdisciplinary reviews Cognitive science*. 10:e1494.
395 30. Santangelo AM, Sawiak SJ, Fryer T, Hong Y, Shiba Y, Clarke HF, et al. (2019): Insula serotonin
396 2A receptor binding and gene expression contribute to serotonin transporter polymorphism anxious
397 phenotype in primates. *Proceedings of the National Academy of Sciences of the United States of America*.
398 116:14761-14768.
399 31. Santangelo AM, Ito M, Shiba Y, Clarke HF, Schut EH, Cockcroft G, et al. (2016): Novel Primate
400 Model of Serotonin Transporter Genetic Polymorphisms Associated with Gene Expression, Anxiety and
401 Sensitivity to Antidepressants. *Neuropsychopharmacology : official publication of the American College*
402 *of Neuropsychopharmacology*. 41:2366-2376.
403 32. Beliveau V, Ganz M, Feng L, Ozenne B, Højgaard L, Fisher PM, et al. (2017): A High-
404 Resolution In Vivo Atlas of the Human Brain's Serotonin System. *The Journal of neuroscience : the*
405 *official journal of the Society for Neuroscience*. 37:120-128.
406 33. Mengod G, Vilaró MT, Cortés R, López-Giménez JF, Raurich A, Palacios JM (2006): Chemical
407 neuroanatomy of 5-HT receptor subtypes in the mammalian brain. *The serotonin receptors*.319-364.
408 34. Robbins TW, Everitt BJ (1996): Neurobehavioural mechanisms of reward and motivation.
409 *Current opinion in neurobiology*. 6:228-236.

410 35. Hillary FG, Grafman JH (2017): Injured Brains and Adaptive Networks: The Benefits and Costs
411 of Hyperconnectivity. *Trends in cognitive sciences*. 21:385-401.
412 36. Di Martino A, Kelly C, Grzadzinski R, Zuo XN, Mennes M, Mairena MA, et al. (2011): Aberrant
413 striatal functional connectivity in children with autism. *Biological psychiatry*. 69:847-856.
414 37. Siegel JS, Ramsey LE, Snyder AZ, Metcalf NV, Chacko RV, Weinberger K, et al. (2016):
415 Disruptions of network connectivity predict impairment in multiple behavioral domains after stroke.
416 *Proceedings of the National Academy of Sciences of the United States of America*. 113:E4367-4376.
417 38. Zhou J, Greicius MD, Gennatas ED, Growdon ME, Jang JY, Rabinovici GD, et al. (2010):
418 Divergent network connectivity changes in behavioural variant frontotemporal dementia and Alzheimer's
419 disease. *Brain : a journal of neurology*. 133:1352-1367.
420 39. Albaugh DL, Smith Y, Galvan A (2020): Comparative analyses of transgene expression patterns
421 after intra-striatal injections of rAAV2-retro in rats and rhesus monkeys: A light and electron microscopic
422 study. *The European journal of neuroscience*. 52:4824-4839.
423 40. Bonaventura J, Eldridge MAG, Hu F, Gomez JL, Sanchez-Soto M, Abramyan AM, et al. (2019):
424 High-potency ligands for DREADD imaging and activation in rodents and monkeys. *Nature*
425 *communications*. 10:4627.
426 41. Nagai Y, Kikuchi E, Lerchner W, Inoue KI, Ji B, Eldridge MA, et al. (2016): PET imaging-
427 guided chemogenetic silencing reveals a critical role of primate rostromedial caudate in reward
428 evaluation. *Nature communications*. 7:13605.
429 42. Roseboom PH, Mueller SAL, Oler JA, Fox AS, Riedel MK, Elam VR, et al. (2021): Evidence in
430 primates supporting the use of chemogenetics for the treatment of human refractory neuropsychiatric
431 disorders. *Molecular therapy : the journal of the American Society of Gene Therapy*.
432 43. Milham M, Petkov C, Belin P, Hamed SB, Evrard H, Fair D, et al. (2021): Toward next-
433 generation primate neuroscience: A collaboration-based strategic plan for integrative neuroimaging.
434 *Neuron*.

435

436 **FIGURE LEGENDS**

437 **Figure 1.** Schematic of experiments. (**A**) An imaging session. Subjects were lightly anesthetized with
438 isoflurane gas throughout a session. A contrast agent (MION, 10 mg/kg) was administered intravenously
439 before functional scans. Drug (vehicle, 0.1 mg/kg DCZ or 0.3 mg/kg DCZ) was prepared and systemically
440 administered (i.v.) following baseline scans, and test scans were acquired after 15 min of drug injection.
441 (**B**) Data analysis pipeline. The scan data for each session initially went through preprocessing procedures.
442 Then seed-based analysis was performed using predetermined ROIs based on the CHARM and SARM
443 atlases. The temporally-concatenated scan data across all sessions was used for ICA.

444

445 **Figure 2.** fMRI based connectome changes after DCZ administration in an example subject. (**A**) CHARM
446 atlas level 3 visualized on an inflated brain (medial view). (**B**) Brain-wide functional connectivity in cortical
447 areas. Confusion matrices represent connectome in baseline scans (left column), test scans (center column),
448 and the difference between test and baseline (right column) for either in the vehicle (top), low-dose DCZ
449 (middle), and high-dose DCZ condition (bottom), respectively. Color indicates z-transformed correlation
450 coefficients. Labels on the right side show ROIs from CHARM atlas. (**C**) SARM atlas level 3 visualized
451 on an inflated brain. (**D**) Confusion matrices for subcortical areas with labels for SARM ROIs on the right
452 side. Conventions are as in *B*.

453

454 **Figure 3.** Group level changes in the fMRI-based connectome following DCZ administration. (**A-C**)
455 Functional connectivity changes in cortical areas. (**A**) Confusion matrices represent differences in z-value
456 (test - baseline) for vehicle (top), low-dose DCZ (middle), and high-dose DCZ (bottom) conditions. Labels
457 on the right side show ROIs from CHARM atlas (level 3). (**B**) Averaged functional connectivity. Bars
458 represent averaged z-value differences for vehicle, low-dose DCZ, and high-dose DCZ conditions. Error

459 bars are standard error. Symbols represent subjects. Asterisk indicates a significant interaction of drug by
460 area category ($p = 0.016$, two-way ANOVA). (**C**) Functional connectivity in each area. Bars indicate
461 averaged z-value differences averaged for each area of the CHARM atlas. Colors indicate frontal (red),
462 parietal (green), temporal (cyan), and occipital areas (yellow) for low-dose (top panel) and high-dose
463 (bottom panel) DCZ conditions. Gray bars indicate vehicle condition. Error bars are standard error.
464 Asterisks indicate significant difference between vehicle and DCZ conditions ($p < 0.01$ with Bonferroni
465 correction, rank-sum test). (**D-F**) Functional connectivity changes in subcortical areas. Conventions are as
466 in *A-C*. Colors in *F* indicate telencephalon (dark red), diencephalon (dark green), mesencephalon (dark
467 blue), metencephalon (dark yellow), and myelencephalon areas (magenta).
468

469 **Figure 4.** Independent component analysis of the effect of high-dose DCZ. (**A-E**) Top panels show
470 independent components (ICs) as correlation coefficients (*r*) on inflated brains. Bottom panels indicate
471 clusters that showed a significant main effect of drug condition ($p < 0.05$, two-way ANOVA).
472

473 **Figure 5.** The impact of systemic DCZ administration on socio-emotional behavior and probabilistic
474 learning. (**A**) The effect of low-dose DCZ in the human intruder task. Bars indicate the mean time spent
475 motionless with systemic administration of vehicle (gray) or low-dose DCZ (light blue) either in alone
476 condition (left panel), profile condition (center panel), or stare condition (right panel). Symbols indicate
477 individual animals. Error bars represent standard error. (**B**) Dosage-dependent changes in reaction time
478 (RT) in the probabilistic learning task. Bar plots represent the mean RT of three subjects in each drug
479 condition (vehicle, low-dose DCZ, high-dose DCZ). Error bars are standard error. Symbols represent
480 individual subjects. Asterisk indicates a significant main effect of drug condition ($p = 2.5 \times 10^{-6}$, one-way
481 repeated-measures ANOVA). (**C**) Relationship between RT and functional connectivity across conditions
482 in the probabilistic learning task. Scatter plots show the RT in each behavioral session (y axis) and the
483 change in overall functional connectivity in a corresponding subject (x axis) for cortical areas (left panel)

484 and for subcortical areas (right panel), respectively. Individual monkeys completed 6-8 behavioral sessions
485 per each condition. The colors represent drug conditions. The solid and dotted lines are linear fitting and
486 confidence intervals, and red lines indicate significant linear correlation between RT and z-value ($p =$
487 0.023).

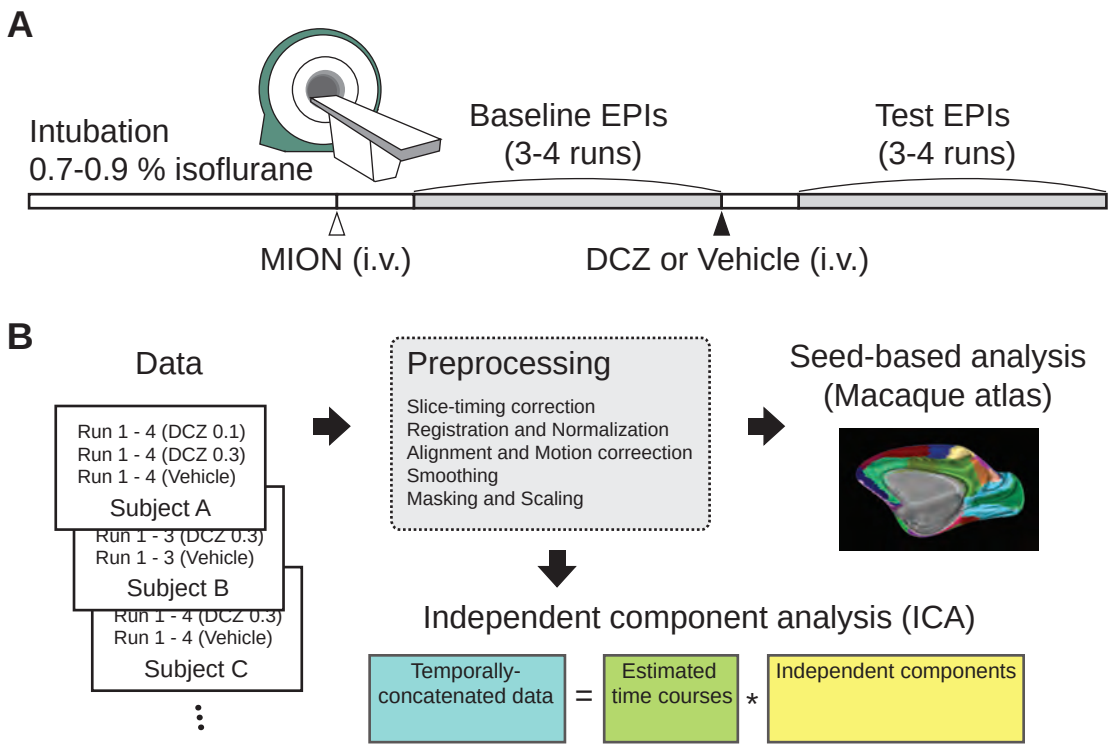
A
Intubation
0.7-0.9 % isoflurane
Baseline EPIs
(3-4 runs)
Test EPIs
(3-4 runs)
MION (i.v.)
DCZ or Vehicle (i.v.)
B
Data
Run 1 - 4 (DCZ 0.1)
Run 1 - 4 (DCZ 0.3)
Run 1 - 4 (Vehicle)
Subject A
Run 1 - 3 (DCZ 0.3)
Run 1 - 3 (Vehicle)
Subject B
Run 1 - 4 (DCZ 0.3)
Run 1 - 4 (Vehicle)
Subject C
Preprocessing
Slice-timing correction
Registration and Normalization
Alignment and Motion correection
Smoothing
Masking and Scaling
Seed-based analysis
(Macaque atlas)
Independent component analysis (ICA)
Temporally-concatenated data
=
Estimated time courses
*
Independent components

FIGURE 1

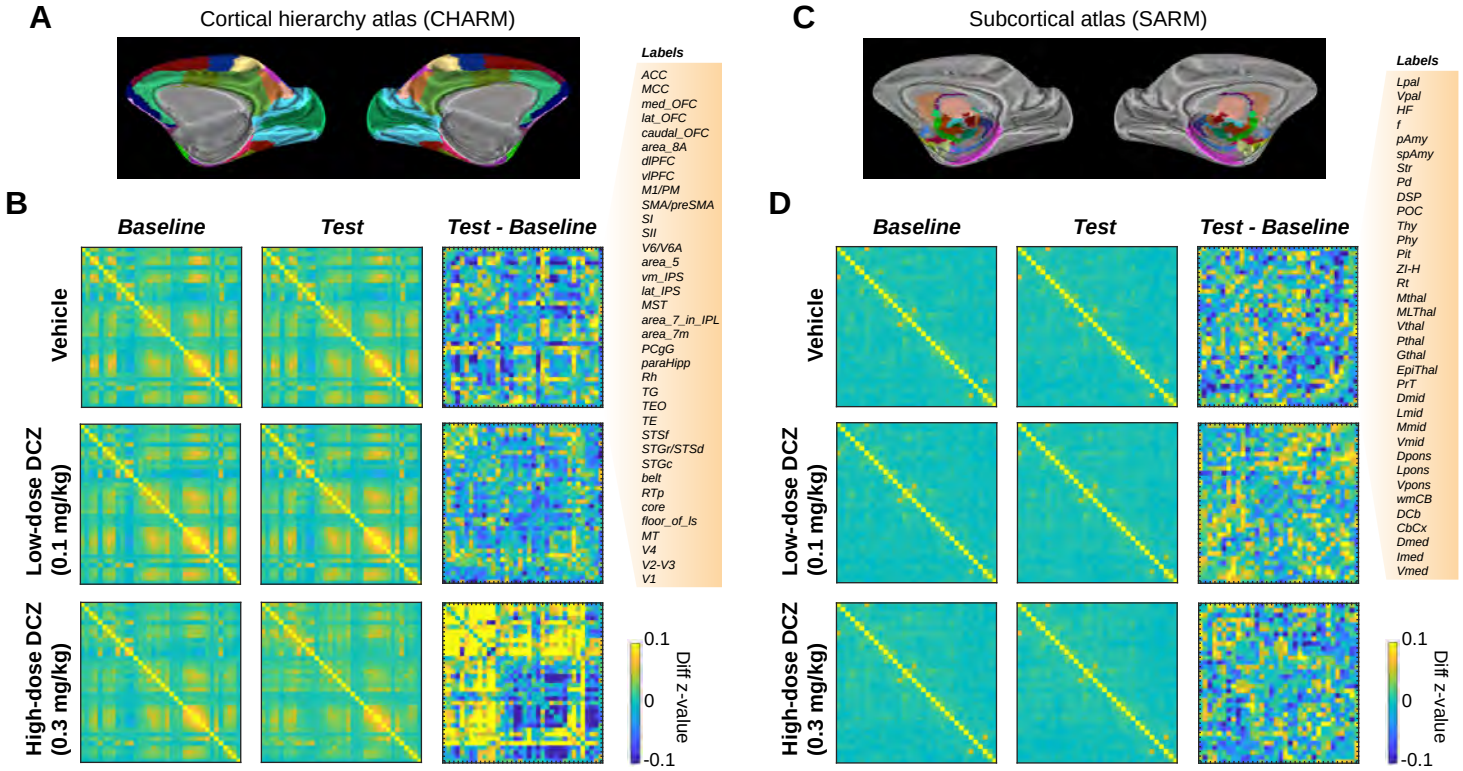
A
Cortical hierarchy atlas (CHARM)
Labels
ACC
MCC
med_OFC
lat_OFC
caudal_OFC
area_8A
dlPFC
vlPFC
M1/PM
SMA/preSMA
SI
SII
V6/V6A
area_5
vm_IPS
lat_IPS
MST
area_7_in_IPL
area_7m
PCgG
paraHipp
Rh
TG
TEO
TE
STSf
STGr/STSd
STGc
belt
RTp
core
floor_of_Is
MT
V4
V2-V3
V1
B
Baseline
Test
Test - Baseline
Vehicle
Low-dose DCZ (0.1 mg/kg)
High-dose DCZ (0.3 mg/kg)
0.1
0
-0.1
Diff z-value
C
Subcortical atlas (SARM)
Labels
Lpal
Vpal
HF
f
pAmy
spAmy
Str
Pd
DSP
POC
Thy
Phy
Pit
ZI-H
Rt
Mthal
MLThal
Vthal
Pthal
Gthal
EpiThal
PrT
Dmid
Lmid
Mmid
Vmid
Dpons
Lpons
Vpons
wmCB
DCb
CbCx
Dmed
Imed
Vmed
D
Baseline
Test
Test - Baseline
Vehicle
Low-dose DCZ (0.1 mg/kg)
High-dose DCZ (0.3 mg/kg)
0.1
0
-0.1
Diff z-value

FIGURE 2

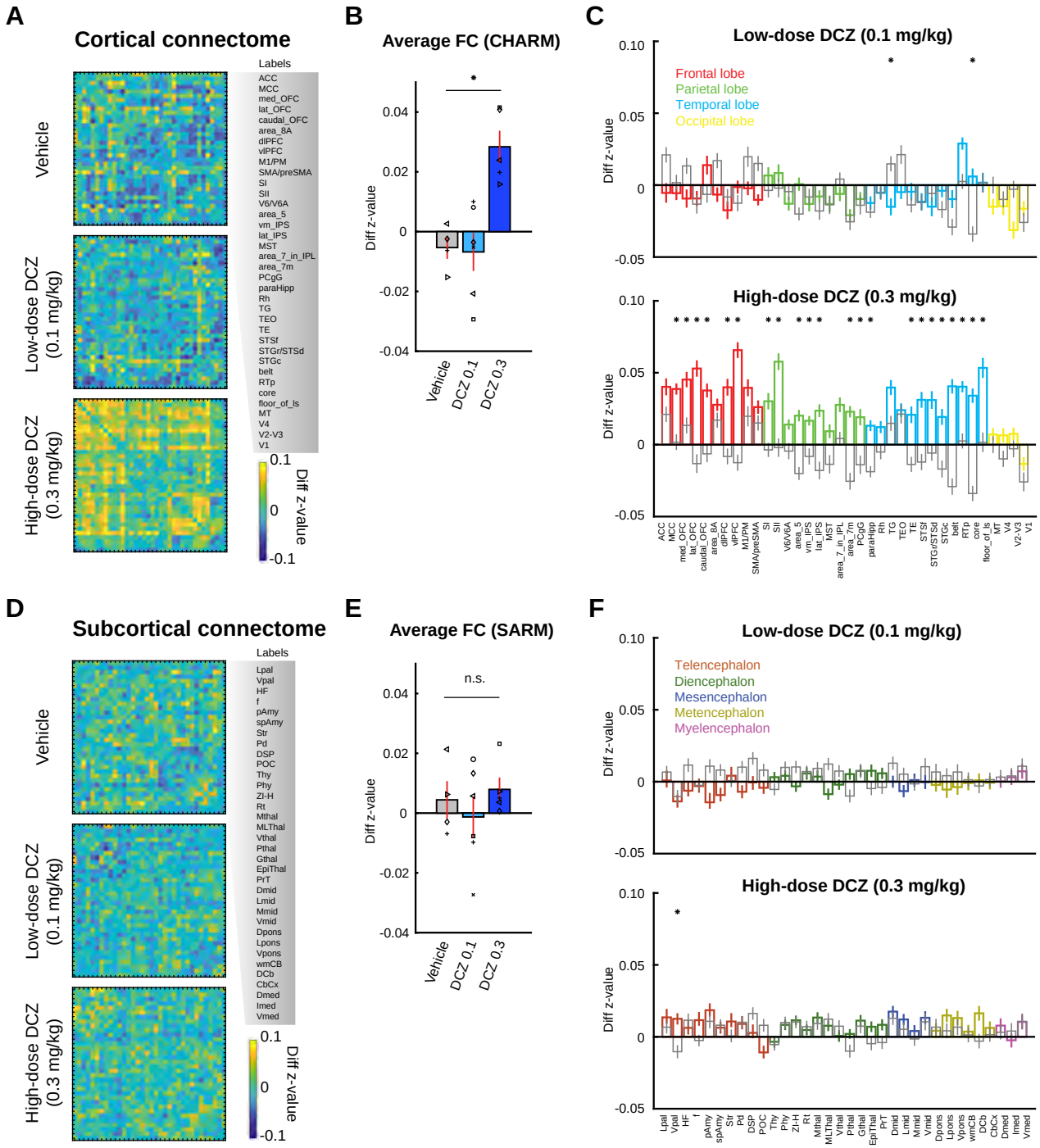
A
Cortical connectome
Vehicle
Low-dose DCZ (0.1 mg/kg)
High-dose DCZ (0.3 mg/kg)
Labels
ACC
MCC
med_OFC
lat_OFC
caudal_OFC
area_8A
dlPFC
vlPFC
M1/PM
SMA/preSMA
SI
SII
V6/V6A
area_5
vm_IPS
lat_IPS
MST
area_7_in_IPL
area_7m
PCgG
paraHipp
Rh
TG
TEO
TE
STSf
STGr/STSd
STGc
belt
RTp
core
floor_of_Is
MT
V4
V2-V3
V1
0.1
0
-0.1
Diff z-value
B
Average FC (CHARM)
*
0.04
0.02
0
-0.02
-0.04
Diff z-value
Vehicle
DCZ 0.1
DCZ 0.3
C
Low-dose DCZ (0.1 mg/kg)
Frontal lobe
Parietal lobe
Temporal lobe
Occipital lobe
0.10
0.05
0
-0.05
Diff z-value
High-dose DCZ (0.3 mg/kg)
D
Subcortical connectome
Labels
Lpal
Vpal
HF
f
pAmy
spAmy
Str
Pd
DSP
POC
Thy
Phy
ZI-H
Rt
Mthal
MLThal
Vthal
Pthal
Gthal
EpiThal
PrT
Dmid
Lmid
Mmid
Vmid
Dpons
Lpons
Vpons
wmCB
DCb
CbCx
Dmed
Imed
Vmed
E
Average FC (SARM)
n.s.
F
Low-dose DCZ (0.1 mg/kg)
Telencephalon
Diencephalon
Mesencephalon
Metencephalon
Myelencephalon
High-dose DCZ (0.3 mg/kg)

FIGURE 3

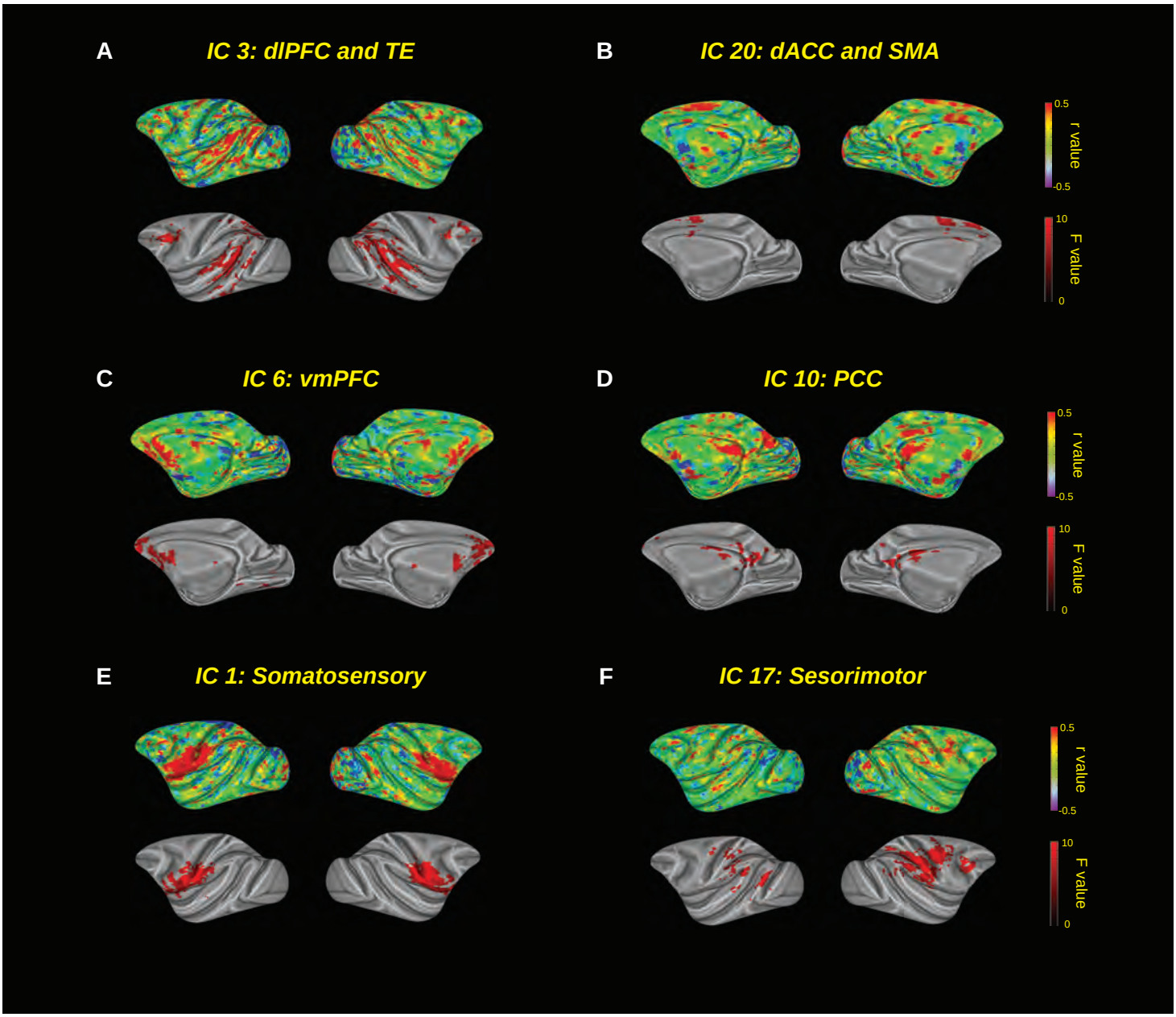
A
IC 3: dlPFC and TE
B
IC 20: dACC and SMA
C
IC 6: vmPFC
D
IC 10: PCC
E
IC 1: Somatosensory
F
IC 17: Sesorimotor
0.5
r value
-0.5
10
F value
0

FIGURE 4

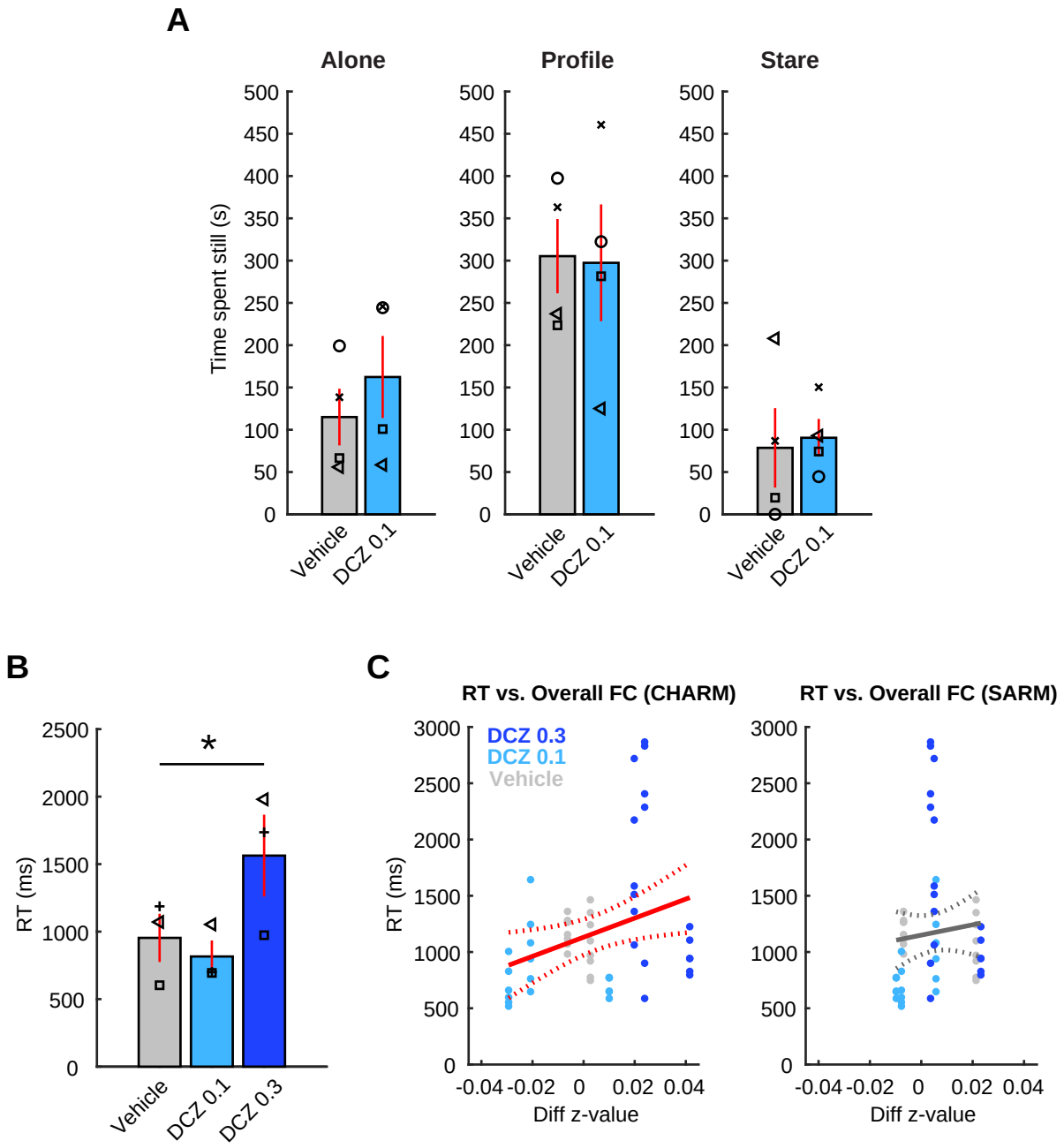
A
Alone
Profile
Stare
Time spent still (s)
500
450
400
350
300
250
200
150
100
50
0
Vehicle
DCZ 0.1
B
RT (ms)
2500
2000
1500
1000
500
0
*
Vehicle
DCZ 0.1
DCZ 0.3
C
RT vs. Overall FC (CHARM)
RT vs. Overall FC (SARM)
DCZ 0.3
DCZ 0.1
Vehicle
3000
-0.04
-0.02
0
0.02
0.04
Diff z-value

FIGURE 5

SUPPLEMENTAL INFORMATION

Title: Resting-state fMRI-based screening of deschloroclozapine in rhesus macaques predicts dosage-dependent behavioral effects

Authors: Atsushi Fujimoto[1]*, Catherine Elorette[1]*, J. Megan Fredericks[1], Satoka H. Fujimoto[1], Lazar Fleysher[4], Peter H. Rudebeck[1+], and Brian E. Russ[1,2,3+y]

Author affiliations:

[1] Nash Family Department of Neuroscience and Friedman Brain Institute, Icahn School of Medicine at Mount Sinai, One Gustave L. Levy Place, New York, NY 10029

[2] Center for Biomedical Imaging and Neuromodulation, Nathan Kline Institute, 140 Old Orangeburg Road, Orangeburg, NY 10962

[3] Department of Psychiatry, New York University at Langone, One, 8, Park Ave, New York, NY 10016

[4] BioMedical Engineering and Imaging Institute, Icahn School of Medicine at Mount Sinai, One Gustave L. Levy Place, New York, NY 10029

* These authors contributed equally to this work

+ Joint last author

y Corresponding author

Correspondence:

Brian E. Russ

brian.russ@mssm.edu

SUPPLEMENTAL METHODS

Drug preparation

To prepare a DCZ solution for fMRI or socio-emotional testing, DCZ powder (HY-42110, MedChemExpress) was dissolved in dimethyl sulfoxide (DMSO, 2% of total volume) and then diluted in saline to a concentration of 0.1 mg/kg or 0.3 mg/kg, with a total volume of 1ml. Vehicle solution was prepared as 2% DMSO diluted in 1ml saline. One vehicle scan was conducted without DMSO (monkey Wo). Both solutions underwent a sterilized filter (0.22 μm) before injection. DCZ or vehicle solution was prepared within 30 min of usage.

For the probabilistic learning testing, both vehicle and DCZ were prepared using sterile procedures and previously published drug preparation approaches for behavioral testing in macaques (1). The vehicle consisted of 0.5% Acetic acid, 50% 1 M Sodium Acetate, and 49.5% 0.2 M NaOH. Each solution of DCZ or vehicle ultimately had a pH between 5.5 and 6.0. When DCZ was administered, the drug was first dissolved in acetic acid and sodium acetate and then diluted with NaOH. The vehicle remained consistent across both drug doses (0.1mg/kg, or 0.3mg/kg of DCZ). However, the concentration of each dose was altered so the total volume of each injection was the same no matter the dose, e.g. a 0.1mg/kg dose had a concentration of 1 mg/mL, while a 0.3 mg/kg dose had a concentration of 3 mg/mL. As with fMRI testing, DCZ or vehicle solution was prepared within 30 min of usage.

fMRI data acquisition

Animals were first sedated with ketamine (5 mg/kg) and dexmedetomidine (0.0125 mg/kg) at least 1.5 hours before the data collection to prevent detrimental effects of ketamine on neural activities. They were then intubated and maintained under low level (0.7-0.8 %) isoflurane throughout the session to ensure preservation of resting-state networks (2). During all scanning sessions, anesthetized macaques were contained within a primate chair in the sphinx position with their heads supported by a sling. Because animals were not held in a stereotactic frame, this meant we were able to maintain sedation with lower levels of anesthesia than is often used. To minimize the effect of physiological changes in the neural activity, vital signs (end-tidal CO2, body temperature, blood pressure, capnograph) were continuously

monitored and maintained as steadily as possible throughout an experimental session. Structural and functional scans were collected each session, as well as pre-injection (baseline) and post-injection (DCZ or vehicle) functional scans. First, a set of setup scans were acquired which included shimming based off the acquired fieldmap. Additionally, a 3D T1-weighted image (0.5 mm isotropic, TR/TE 2500/2.81 ms, flip angle 8°) was acquired. Following MION injection (i.v.) (3, 4), three to four runs of echo planar image (EPI) functional scans (1.6 mm isotropic, TR/TE 2120/16 ms, flip angle 45°, 300 volumes per each run) were obtained for baseline functional resting states. Then, either DCZ (0.1 or 0.3 mg/kg) or vehicle was administered (i.v.), and subsequently an additional three to four functional runs (with the same parameters) were collected. Test EPI data were collected approximately 15 minutes after DCZ or vehicle injection to ensure trafficking of the drug to the brain (5).

Unconditioned socio-emotional tasks

Four animals (Wo, He, La, Ha) were tested on two well validated behavioral tasks that assess socio-emotional function: the human intruder (6) and social interaction tests (7). Behavioral tests were conducted following injections of either vehicle (2% DMSO in saline) or 0.1 mg/kg DCZ. Injections were given intramuscularly (i.m.) 30-60 minutes before behavioral testing in keeping with the known pharmacokinetics of DCZ. Experiments were counterbalanced for treatment order among animals. All behavioral data were scored offline in Observer XT (Noldus, Wageningen, the Netherlands).

<u>Human Intruder:</u> Animals were tested on a human intruder paradigm, which has been shown to accurately assess anxiety behaviors in macaques (6, 8-10). Testing was conducted in a Wisconsin General Testing Apparatus (WGTA). The sliding doors of the WGTA were left open so the animal could observe the room throughout the test session. We have adapted our testing procedure and behavioral ethogram from a previous study (11).

The paradigm consisted of three conditions (alone, profile, stare) presented in the same order to all monkeys for a total duration of 30 min. The experimenter wore a rubber mask depicting a different human male face during each testing session, presented in pseudorandom order to subjects with no repetitions of masks per subject. Different colored curtains hung behind the experimenter's seat were also used to increase novelty.

77 Within each testing session, monkeys were first left alone to observe the room and acclimatize to the
78 environment (alone condition). Next, the experimenter, wearing a novel mask, stepped into the animal's
79 field of view with only their profile visible to the animal. The experimenter remained still, with only the
80 profile visible, for 9 minutes (profile condition). Another alone condition elapsed for 3 minutes in order to
81 allow the animal to return to baseline behavior, before the experimenter stepped back into view facing the
82 animal and making eye contact. The experimenter remained still, attempting to make eye contact with the
83 animal for 9 minutes (stare condition) before stepping out of view and ending the session.
84 Social Interaction: Animals were removed from the home cage and placed in a play cage set up in an
85 unfamiliar room. A familiar cagemate was introduced to the play cage, and social interaction between the
86 subject and cagemate was observed. We used an ethogram previously defined by others to evaluate social
87 behaviors (12, 13). The cagemate chosen for this task was always the same across conditions.
88 *Probabilistic stimulus-reward learning task*
89 Three monkeys (He, Cy, and Wo) were trained to perform a two alternative forced choice probabilistic
90 learning task on a touch-sensitive monitor. All testing occurred while monkeys were seated in a wheeled
91 transport cage. In each 200-trial session, subjects had to learn to discriminate which visual stimulus in
92 two pairs of novel stimuli was associated with the highest probability of receiving a food reward pellet
93 (banana, grape, and raspberry flavored 20mg BIO-Serv Dustless Precision Pellets®). In each pair of
94 stimuli, one option was associated with an 80% probability of receiving a reward whereas the other was
95 associated with 20% probability of receiving a reward. Stimuli were novel at the beginning of each
96 session, the assignment of visual stimuli to high/low probability was random, and the probability of
97 receiving a reward was fixed throughout the session.
98 Each trial began with the presentation of a centrally located green square 'lever' stimulus. Once monkeys
99 pressed the lever stimulus, two stimuli were presented to the left and right of the screen, and monkeys
100 could choose between them. Pressing one stimulus caused the non-selected option to be removed from the
101 screen. The chosen stimulus remained on the screen for a further 0.5 seconds before being extinguished
102 and a 4 second inter-trial interval commenced. For one pair of stimuli, if a reward was to be delivered it

was dispensed when the chosen stimulus was removed from the screen. For the other pair of stimuli if a reward was to be delivered, it was dispensed 1 second after the chosen stimulus was removed from the screen. The presentation of stimuli pairs was randomized across trials and the left-right location of each stimulus was also counterbalanced across trials.

Monkeys completed daily 200-trial sessions (100 trials of each pair), run 4-5 days per week. 0.1mg/kg, 0.3mg/kg DCZ, and vehicle were administered in sessions after stable performance was established each week. In practice this meant that injections of 0.1mg/kg, 0.3mg/kg DCZ, or vehicle were administered on either Wednesday, Thursday, or Friday.

fMRI analysis

Functional imaging data was preprocessed with standard AFNI/SUMA pipelines (14, 15). Raw images were first converted into NIFTI data file format and ordered into BIDS format (16). The T1 weighted image from each session was first warped to the standard NMT atlas space using a newly developed macaque skull stripping function followed by AFNI's @animal_warper command (15, 17). Specifically, the T1w images were spatially normalized, then skull stripped using the U-Net model built from Primate Data-Exchange open data sets (18), the mask was dilated out 6mm to ensure the whole brain was within the mask, and finally the mask was applied to the original image, which was then renormalized. This normalized skull-stripped T1w image was then aligned to the NMT atlas (17), along with subject specific versions of the CHARM (15) and SARM atlases (19).

The EPI data were preprocessed using a customized version of the AFNI NHP preprocessing pipeline (Jung et al 2020). For each session pre- and post-injection data were processed separately using the same parameters. In addition to a set of dummy scans, the first 3 TRs of each EPI were removed to ensure that any magnetization effects were removed from the data prior to functional connectivity analyses. The images were first slice time corrected, then motion correction was applied and the EPIs were aligned to the within session T1w image and warped to the standard space. Following alignment to the standard space, the EPIs were blurred with a full width half max of 3mm, and then converted to percent signal change. We then regressed the motion derivatives from each scan along with CSF and WM signal

129 regressors. The residuals of this analysis were then used to compute the functional connectivity analysis
130 described below.
131 The full connectome analyses were computed using 3dNetCorr function in AFNI (14, 20). The error time
132 series from the preprocessing steps described above were split into half runs and then we computed the
133 correlation between ROIs at various levels of the cortical (15) and subcortical (19) hierarchical atlas.
134 Following the creation of the individual correlation matrices, or connectomes, for each half run, the
135 connectomes were Fisher's z-transformed and then averaged within condition to create mean
136 connectomes for each condition (both pre-/post- injection for the vehicle, DCZ 0.1 mg/kg, and DCZ 0.3
137 mg/kg sessions) at all hierarchical levels. We then calculated the difference between connectomes by
138 subtracting the pre-injection data from the post- injection data for each session. Finally the average
139 difference connectome was computed across subjects for each drug level. To statistically determine the
140 effect of drug on the functional connectivity in CHARM and SARM atlases, the mean connectomes from
141 individual monkeys were then submitted to an ANOVA with main effects of drug and area category.
142 Monkey and brain area were modeled as random effects and brain area was nested under monkey.
143 In addition to the functional connectomes analyses, we used a modified group Independent Components
144 Analysis (ICA) to look for any changes in the component structure of our data following the drug
145 manipulations. The same split run error time series from the connectome analyses were submitted to
146 FSL's melodic ICA function (21, 22) allowing for 30 possible components and a mixture model threshold
147 of 0.5. Following the computation of the group ICA, we submitted resultant data to FSL's dual regression
148 function, which was used to extract the spatial ICs for each subject and condition (21, 23). The extracted
149 condition IC scores were then submitted to a 2 (Pre-Injection vs Post-Injection) by 3 (Drug: Vehicle, DCZ
150 0.1 mg/kg, DCZ 0.3 mg/kg) ANOVA which was computed on a voxel by voxel basis.
151 *Behavioral analysis*
152 Data from socio-emotional tests were assessed by a scorer blinded to the condition. Data was scored in
153 Observer XT and exported to GraphPad Prism (GraphPad, San Diego CA). Behavioral ethograms
154 (**Supplemental Tables 2** and **3**) were adapted from previous studies (11, 13). Behavioral responses in the

human intruder and social interaction paradigms were assessed for normality using a Shapiro-Wilk normality test. Human intruder data was analyzed using two-way repeated measures ANOVAs with matching by subject. No assumption of sphericity was made. Sidak's multiple comparison test was used to evaluate differences between categories (i.e. differences between DCZ and vehicle treatments within the alone, profile, and stare conditions). Social interaction data was analyzed using a paired student's t-test, with matching by subject.

Data from the probabilistic learning task was analyzed using MATLAB. In all sessions analyzed, each of the monkeys learned to discriminate the pairs of stimuli by the end of the session. This was based on a running average of 10 trials and criterion was set at 8/10 trials or 80%. We assessed reaction time (RT) as a measure of general task-execution process such as attention or motivation. RT was defined as the time duration (in milliseconds) from the presentation of two stimuli to a choice response of the monkeys. We analyzed RT using ANOVA with factors of drug as a main effect and monkey and session as random effects.

SUPPLEMENTAL TABLES

Animal	rs-fMRI (vehicle)	rs-fMRI (DCZ 0.1 mg/kg)	rs-fMRI (DCZ 0.3 mg/kg)	Socio-emotional tasks	Probabilistic learning task
La	N	Y	N	Y	N
Ha	Y	Y	N	Y	N
Wo	Y	Y	Y	Y	N
He	N	Y	Y	Y	Y
Cy	Y	Y	Y	N	Y
Bu	Y	Y	Y	N	Y
Pi	Y	N	Y	N	N

Supplemental Table 1: Assignments of monkeys to fMRI and behavioral testing conditions. Y and N indicate the condition that the data was collected and not collected, respectively.

Category and Specific Behaviors	Measurement	Examples
Affiliative	Cumulative Frequency	
Lipsmack	Frequency	Rapid movement of pursed lips, accompanied by a smacking sound
Present	Frequency	Rigid posture (knees locked) with tail elevated and rump oriented toward the stimulus object
Anxiety	Cumulative Frequency	
Scratch	Frequency	Rapid scratch of body with hands or feet
Body shake	Frequency	Shake of the whole body or just head and shoulders region
Tooth grind	Frequency	Repetitive rubbing or chewing of upper and lower teeth
Yawn	Frequency	Open mouth widely, exposing teeth
Fearful	Cumulative Frequency	
Withdrawal	Frequency	Quick, jerky motion away from the stimulus object (jump back)
Grimace	Frequency	Retracted lips, exposed clenched teeth
Hostile	Cumulative Frequency	
Cage aggression	Frequency	Slaps, shakes, bites, or slams body against cage
Threat	Frequency	Open mouth (no teeth exposed)
Bark	Frequency	Low pitch, high intensity, rasping, guttural
Lunge	Frequency	A quick, jerky movement toward the stimulus
Position	Duration	
Front of cage	Duration	No part of animal's body contacts back of the cage

Back of cage	Duration	Animal's body contacts back of the cage
Stereotypies	Cumulative Duration	
Pacing	Duration	Repetitive motor pattern around the test cage
Motor Stereotypy	Duration	Repetitive, abnormal voluntary or involuntary motor patterns (e.g. swinging, twirling, flipping)
Stillness	Duration	Motionless posture for at least 3 seconds (except small head movements)
Vocalizations	Cumulative Frequency	
Coo	Frequency	Clear soft pitch and intensity, sounds like "ooooh"
Scream	Frequency	High pitch, high intensity screech or loud chirp

Supplemental Table 2. Behavioral ethogram for human intruder task, adapted from Raper et al. 2019.

Category and Specific Behaviors	**Measurement**	**Examples**
Avoidance	Cumulative Frequency	
Attack	Frequency	Makes threatening gestures (i.e., mouth threat, head or body lunge, cage shake) towards or hits, grabs or bites the conspecific
Cower	Frequency	Withdraws from the conspecific in a crouched or recoiled position
Escape	Frequency	Sudden, explosive movement away from conspecific
Withdrawal	Frequency	Moves away at a normal pace from the conspecific when approached
Movement	Cumulative Duration	
Passive	Duration	Inactive, stays in one location
Manipulation	Duration	Handles, chews, licks, moves, or smells objects or cage parts
Locomotion	Duration	Walks, runs, climbs, or jumps
Self-directed	Duration	Engages in self-directed behaviors

Social Contact	Cumulative Duration	
Contact	Duration	Touches or holds the conspecific, not covered by any other behavior
Gives grooming	Duration	Subject grooms the conspecific
Receives grooming	Duration	The conspecific grooms the subject
Play	Duration	Chasing, wrestling, and "rough and tumble" behaviors

Supplemental Table 3. Behavioral ethogram for social interaction task, adapted from Forcelli et al. 2017.

SUPPLEMENTAL REFERENCES

1. Upright NA, Baxter MG (2020): Effect of chemogenetic actuator drugs on prefrontal cortex-dependent working memory in nonhuman primates. *Neuropsychopharmacology : official publication of the American College of Neuropsychopharmacology*. 45:1793-1798.
2. Wu TL, Mishra A, Wang F, Yang PF, Gore JC, Chen LM (2016): Effects of isoflurane anesthesia on resting-state fMRI signals and functional connectivity within primary somatosensory cortex of monkeys. *Brain and behavior*. 6:e00591.
3. Russ BE, Petkov CI, Kwok SC, Zhu Q, Belin P, Vanduffel W, et al. (2021): Common functional localizers to enhance NHP & cross-species neuroscience imaging research. *NeuroImage*. 237:118203.
4. Leite FP, Tsao D, Vanduffel W, Fize D, Sasaki Y, Wald LL, et al. (2002): Repeated fMRI using iron oxide contrast agent in awake, behaving macaques at 3 Tesla. *NeuroImage*. 16:283-294.
5. Nagai Y, Miyakawa N, Takuwa H, Hori Y, Oyama K, Ji B, et al. (2020): Deschloroclozapine, a potent and selective chemogenetic actuator enables rapid neuronal and behavioral modulations in mice and monkeys. *Nature neuroscience*. 23:1157-1167.
6. Kalin NH, Shelton SE (1989): Defensive behaviors in infant rhesus monkeys: environmental cues and neurochemical regulation. *Science (New York, NY)*. 243:1718-1721.
7. Kling A, Cornell R (1971): Amygdalectomy and social behavior in the caged stump-tailed macaque (Macaca speciosa). *Folia primatologica; international journal of primatology*. 14:190-208.

195 8. Kalin NH, Shelton SE, Davidson RJ, Kelley AE (2001): The primate amygdala mediates acute
196 fear but not the behavioral and physiological components of anxious temperament. *The Journal of*
197 *neuroscience : the official journal of the Society for Neuroscience*. 21:2067-2074.
198 9. Izquierdo A, Newman TK, Higley JD, Murray EA (2007): Genetic modulation of cognitive
199 flexibility and socioemotional behavior in rhesus monkeys. *Proceedings of the National Academy of*
200 *Sciences of the United States of America*. 104:14128-14133.
201 10. Kalin NH, Shelton SE, Davidson RJ (2007): Role of the primate orbitofrontal cortex in mediating
202 anxious temperament. *Biological psychiatry*. 62:1134-1139.
203 11. Raper J, Murphy L, Richardson R, Romm Z, Kovacs-Balint Z, Payne C, et al. (2019):
204 Chemogenetic Inhibition of the Amygdala Modulates Emotional Behavior Expression in Infant Rhesus
205 Monkeys. *eNeuro*. 6.
206 12. Wellman LL, Forcelli PA, Aguilar BL, Malkova L (2016): Bidirectional Control of Social
207 Behavior by Activity within Basolateral and Central Amygdala of Primates. *The Journal of*
208 *neuroscience : the official journal of the Society for Neuroscience*. 36:8746-8756.
209 13. Forcelli PA, Wellman LL, Malkova L (2017): Blockade of glutamatergic transmission in the
210 primate basolateral amygdala suppresses active behavior without altering social interaction. *Behavioral*
211 *neuroscience*. 131:192-200.
212 14. Cox RW (1996): AFNI: software for analysis and visualization of functional magnetic resonance
213 neuroimages. *Computers and biomedical research, an international journal*. 29:162-173.
214 15. Jung B, Taylor PA, Seidlitz J, Sponheim C, Perkins P, Ungerleider LG, et al. (2021): A
215 comprehensive macaque fMRI pipeline and hierarchical atlas. *NeuroImage*. 235:117997.
216 16. Gorgolewski KJ, Auer T, Calhoun VD, Craddock RC, Das S, Duff EP, et al. (2016): The brain
217 imaging data structure, a format for organizing and describing outputs of neuroimaging experiments.
218 *Scientific data*. 3:160044.
219 17. Seidlitz J, Sponheim C, Glen D, Ye FQ, Saleem KS, Leopold DA, et al. (2018): A population
220 MRI brain template and analysis tools for the macaque. *NeuroImage*. 170:121-131.

221 18. Wang X, Li XH, Cho JW, Russ BE, Rajamani N, Omelchenko A, et al. (2021): U-net model for
222 brain extraction: Trained on humans for transfer to non-human primates. *NeuroImage*. 235:118001.
223 19. Hartig R, Glen D, Jung B, Logothetis NK, Paxinos G, Garza-Villarreal EA, et al. (2021): The
224 Subcortical Atlas of the Rhesus Macaque (SARM) for neuroimaging. *NeuroImage*. 235:117996.
225 20. Taylor PA, Saad ZS (2013): FATCAT: (an efficient) Functional and Tractographic Connectivity
226 Analysis Toolbox. *Brain connectivity*. 3:523-535.
227 21. Beckmann CF, Mackay CE, Filippini N, Smith SM (2009): Group comparison of resting-state
228 FMRI data using multi-subject ICA and dual regression. *NeuroImage*. 47:S148.
229 22. Beckmann CF, Smith SM (2004): Probabilistic independent component analysis for functional
230 magnetic resonance imaging. *IEEE transactions on medical imaging*. 23:137-152.
231 23. Nickerson LD, Smith SM, Öngür D, Beckmann CF (2017): Using Dual Regression to Investigate
232 Network Shape and Amplitude in Functional Connectivity Analyses. *Frontiers in neuroscience*. 11:115.